Available online at www.sciencedirect.com
ScienceDirect
Catalysis Today 131 (2008) 3–14
CATALYSIS TODAY
www.elsevier.com/locate/cattod

Preparation and photocatalytic activity of nanotubes obtained from titanium dioxide

M. Qamar [a,b], C.R. Yoon [a], H.J. Oh [a], N.H. Lee [a], K. Park [a], D.H. Kim [c], K.S. Lee [c], W.J. Lee [d], S.J. Kim [a,*]

[a] *Institute/Faculty of Nanotechnology and Advanced Materials Engineering, Sejong University, #98 Gunja-dong, Gwangjin-gu, Seoul 143-747, Republic of Korea*
[b] *Department of Chemistry, Aligarh Muslim University, Aligarh 202002, India*
[c] *Department of Advanced Materials Engineering, Hanyang University, Haengdang-dong, Seondong-gu, Seoul 133-791, Republic of Korea*
[d] *Korea Electrotechnology Research Institute, #28-1 Sungju-Dong, Changwon, Gyeongnam 641-120, Republic of Korea*

Available online 26 November 2007

Abstract

The TiO_2 sol was prepared hydrothermally in an autoclave from aqueous $TiOCl_2$ solutions using as a starting precursor. Titanate nanotubes were obtained when the sol–gel-derived TiO_2 sol was treated chemically with a 10 M NaOH solution and subsequently heated in the autoclave at 150 °C for 48 h. The samples were characterized using XRD, TEM, SEM, EDX, FT-IR, and BET surface area analyzer. The experimental results revealed that the phase, shape and morphology, surface property and the photocatalytic activity were greatly affected by the calcination temperatures and amount of sodium present in the different samples. On the basis of different experimental evidences, formula $Na_2Ti_3O_7{\cdot}nH_2O$, $Na_{2-x}H_x$-$Ti_3O_7{\cdot}nH_2O$ and $H_2Ti_3O_7{\cdot}nH_2O$ has been proposed for the nanotubes depending on the extent of exchange reaction of sodium with proton. A systematic study, dealing with the photocatalytic activity of the titanate nanotubes, was also carried out as a function of sodium contents and calcination temperatures. The photocatalytic activity of samples, obtained before and after calcination containing different amounts of sodium, was evaluated using the photooxidation of a dye, amaranth, as probe reaction. The as-prepared nanotubes, with or without sodium contents, showed no photocatalytic activities but when the samples containing partial or without sodium ions were heated at different temperatures, photocatalytic activity was drastically increased following the change in phase.

Keywords: TiO_2; Titanates; Nanotubes; Hydrothermal process; Photocatalytic activity

1. Introduction

Nanotubes are ubiquitous in the world of science. Recently, a number of nanotubes, made of materials other than carbon, have attracted the attention of many inorganic chemists. Delving into the periodic table, these scientists are finding that nanotubes made from inorganic materials have intriguing properties quite different from those of their all-carbon cousins and a range of potential applications. Of such materials, titanates nanotubes have received a great deal of attention, in part because TiO_2 can exhibit a wealth of important photovoltaic (solar energy conversion), photocatalytic, semiconductor, catalytic support, and gas sensing properties, especially when prepared in a nanomaterial. In addition, these materials can serve as low-voltage intercalation hosts for lithium and, hence, as cathodes for rechargeable lithium ion batteries or supercapacitors [1–6]. Research on TiO_2 includes nanoparticles [7], thin films [8], and mesoporous TiO_2 [9]. The nanotubes derived from TiO_2 with diameters of 70–100 nm were produced using a sol–gel method [10] or porous alumina as a template [11]. Smaller nanotubes with diameters of about 8 nm were also reported, and the structure of the tube was confirmed to be anatase [12], anatase–rutile [13], or layered hydrogen titanate [14]. Following the discovery of nanotube morphology in carbon, a wide variety of layered materials have been shown to be able to form nanotubes [15]. However, the mechanism of formation and the method of regulating the morphologies (diameter and length, wall thickness, size

* Corresponding author.
E-mail address: sjkim1@sejong.ac.kr (S.J. Kim).

0920-5861/$ – see front matter © 2007 Elsevier B.V. All rights reserved.
doi:10.1016/j.cattod.2007.10.015

distribution, and the sizes of nanotube agglomerates) of the various types of nanotubes are still the subject of intense research. Mainly, three approaches have been reported for the preparation of these tubular materials in powdery forms: the template method [16], the anodic oxidation [17], and the wet chemical method [12]. The hydrothermal process, as a wet chemical method, has been used to obtain layered nanostructures.

A simple and cost-effective hydrothermal method for the large-scale production of nanotubular material was proposed by Kasuga et al. [12]. The formation mechanism and phase of resulting nanotubes are still an issue of debate. Different crystal structures and compositions have been presented to describe the nanotubes structure, such as trititanate ($H_2Ti_3O_7$) [14,18–20], tetratitanate $H_2Ti_4O_9{\cdot}H_2O$ [21], lepidocrocite titanate $H_xTi_{2-x/4}\square_{x/4}O_4$ [22,23], $H_2Ti_3O_7{\cdot}xH_2O$ [24], $Na_xH_{2-x}Ti_3O_7$ [25–27], $H_2Ti_2O_4(OH)_2$ [28], and TiO_2 anatase [12,29–31]. In this connection, the products obtained after thermal decomposition of the nanotubes can provide strong evidences about its original crystal structure. In this paper, a detailed study, therefore, has been performed to evaluate the crystal structure of the nanotubes by means of thermal products obtained after heating the nanotubes containing different ratio of sodium ions.

Although one of the most important applications of the titanate nanotubes may be in photocatalysis, a little data is present in the literature dealing with the photocatalytic activity of nanotubes. Even in the little amount of literature, there are many crucial uncertainties regarding the photocatalytic property of the titanate nanotubes. For example, few researchers insist that the as-prepared (sodium titanates) or hydrogen titanates nanotubes have enough potential to degrade the organic pollutants efficiently [21,31–33]. In contrast, few researchers believe that neither of the samples (sodium or hydrogen titanate nanotubes) can be used as a photocatalyst because they found that these samples are inert towards photocatalytic reactions [34–37]. The later studies indicated that the as-prepared nanotubes or treated with acid do not show any photocatalytic activity but the photocatalytic activity increases when these samples are calcined at different temperatures. The controversy extended when the photocatalytic property of calcined nanotubes were compared with commercial powders namely anatase or Degussa P25. For instance, Yu et al. [35] reported that the calcined samples of nanotubes showed higher photocatalytic activity than Degussa P25 by a factor of about 3.0 times. In contrast, Zhang et al. [34] claimed that the photocatalytic activity of the samples of the nanotubes heated at different temperatures was found to be lower than that of commercially available powders.

One of the important factors responsible for different photocatalytic activity of the nanotubes may be the amount of sodium contents present in the samples because the sodium ions present in the samples obtained after hydrothermal process may play a crucial role in phase change and shape and morphology as a function of calcination temperatures. A systematic study, therefore, has also been carried out to see the effect of different calcination temperatures as a function of sodium contents or vice-versa on the photocatalytic activity of nanotubes which in turn is affected by the resulting phase, shape and morphology, BET surface area and so on.

2. Experimental

2.1. Preparation of the samples

The process describing the preparation of TiO_2 precursor is thoroughly discussed in literature [38]. To prepare TiO_2 sol, we heated the TiO_2 precursor in an autoclave reactor (internal capacity of 500 ml) at 150 °C by applying pressure (N_2, 100 BAR) for 5 h. A small amount of obtained TiO_2 sol was then chemically treated with 10 M NaOH concentration. After stirring, the resulting solution was transferred to a Ni lined autoclave and was heated at 150 °C for 48 h. The obtained white product was divided in to three parts. First part was washed only with deionized water and termed as sample A. However, the second part (sample B) was washed with acid (0.1 N HCl) in such a way that it contains a little amount of sodium ions and the third part was washed with acid (0.1 N HCl) repeatedly for a long time at 40 °C in order to remove the sodium ions completely and the sample free from sodium was termed as sample C. The washing of the samples involved stirring the sample in an acid solution followed by a rinsing by deionized water until the solution was found to be free from remaining chloride ions. After filtration, the sample was subjected to freeze drying process at −57 °C to obtain the dried powder and then calcined at different temperatures between 300 and 900 °C for 2 h in the air.

2.2. Characterization methods

The characterization of these samples was carried out by employing various techniques, such as transmission electron microscopy (TEM, JEOL-2010), scanning electron microscopy (SEM, Hitachi S-4700), energy dispersive X-ray spectroscopy (EDX, attached to the SEM), powder X-ray diffraction (XRD, with Cu Kα radiation, Simens-D50050D), Fourier Transform Infrared spectroscopy (FT-IR, Nicolet 380) and Brauner–Emmett–Teller surface area analysis (BET, KICT-SPA3000). FT-IR spectra were recorded with 4 cm^{-1} resolution for 100 scans. The anatase crystallite size of the samples was determined by means of Debye–Scherrer equation using the main diffraction peak for anatase (101).

2.3. Evaluation of photocatalytic activity

The photocatalytic activity of the different samples was evaluated using a beaker made of Pyrex glass equipped with a magnetic stirring bar. For irradiation experiments, 500 ml solution of the dye (amaranth) of 0.15 mM concentration was taken into the vessel and required amount of the catalyst (1 g l^{-1}) was added into the solution. Before irradiation, the solution was magnetically stirred for 30 min to allow the equilibration of the system so that the loss of compound due to adsorption can be taken into account. The zero time reading was obtained from blank solution kept in the dark but otherwise

treated similarly to the irradiated solution. Irradiations were carried out using UV-lamp and samples were collected before and at regular intervals during the irradiation.

The degradation rate for the decomposition (decrease in absorption intensity vs. irradiation time) of the dye under investigation was monitored by measuring the change in absorbance on a UV-Vis spectrophotometer (Scinco Co.). The absorbance of the amaranth (0.15 mM) was followed at 517.9 nm wavelength. For each experiment, the rate constant was calculated from the initial slope obtained by linear regression from a plot of the natural logarithm of the absorbance of the dye as a function of irradiation time. The degradation rates were calculated in terms of [M min^{-1}]. The percent photonic efficiency was calculated using the following equation:

$$\zeta(\%) = \frac{(-dC/dt)_{t=0}}{\text{light intensity}} \times 100$$

where ζ = photonic efficiency, $(-dC/dt)_{t=0}$ is the initial degradation rate assuming first order kinetics, light intensity was found to be 0.576 W/m^2

3. Results and discussion

3.1. Influence of sodium ions

The chemical composition and the respective percentage of each atom present in the samples, obtained after different post treatments, were analyzed by EDX (not shown here). The results obtained for samples A, B and C indicated that the quantity of sodium in sample A is much higher (7.08 wt%) than that of sample B (1.09 wt%) and the amount of sodium in sample C was found to be less than the instrument can detect. The results indicated that a complete removal of sodium ions from the as-prepared samples can be obtained by washing the sample for a long time with 0.1 N HCl at some temperature like 40 °C.

The XRD patterns of the starting material and of the three samples A, B and C together with reflections (bars) from $Na_2Ti_3O_7$ and TiO_2 (anatase) are shown in Fig. 1. The washing of the obtained nanotubes with acid shows significant effect on the crystalline qualities and phase of the samples. The patterns of the nanotubes are significantly different from the structure of the precursor TiO_2 sol (anatase). The XRD patterns of the nanotubes obtained after washing with hydrochloric acid (samples B and C) are different from those obtained after washing only with deionized water (sample A). It seems that the intensities of the peaks around 10° and 28° (corresponding to interlayer spacing) are decreasing as a function of acid washing and these intensities are significantly weakened for the sample C which indicates the change in structure. This change may arise due to the ion-exchange reaction where the interlayer sodium ions are substituted by protons and, hence, a decrease in the interlayer spacing (due to smaller size of hydrogen) may be expected that was indicated by a decrease in the intensity around 10°.

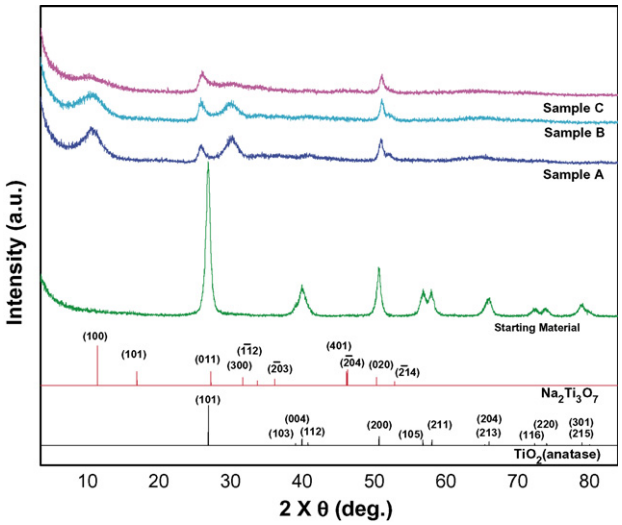

Fig. 1. Comparative XRD patterns of the starting material and titanate nanotubes containing different sodium ions together with reflections (bars) from $Na_2Ti_3O_7$ and TiO_2 (anatase).

Study of samples A and C of the nanotubes was also followed by FT-IR in the range between 4000 and 400 cm^{-1} and the results obtained have been illustrated in Fig. 2. When the IR spectra of the nanotubes (samples A and C) were compared with those reported in the literature for original samples of $Na_2Ti_3O_7$ and $H_2Ti_3O_7$ [41,42], the set of observed bands and spectrum features agrees fairly well within the range studied. The differences in peak intensities and broadening of the peaks between the original samples and nanotubes may be due to the dimensional confinement possessed by nanotubes. The FT-IR spectra of the samples A and C showed broad and intense bands located at around 3375.25, 1637.58, and 897 cm^{-1}. The positions of the bands of both the samples were more or less similar but for sample A, the band around 897 cm^{-1} was prominent (the view showing this band is more obvious in the figure inserted). A broad and intense band located around 3400–3200 cm^{-1} can be ascribed to OH-stretching vibrations. The presence of this peak advocates the

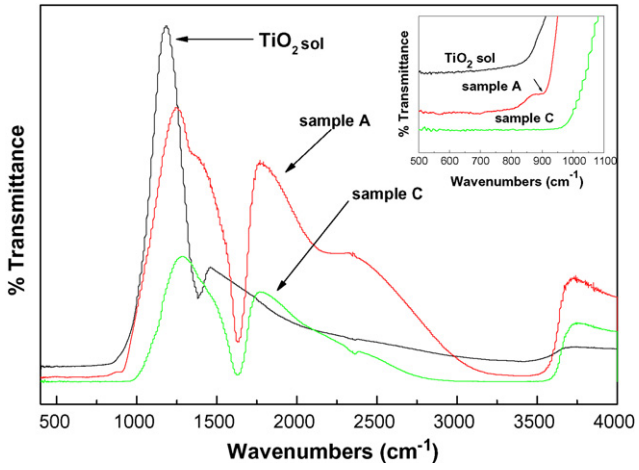

Fig. 2. FT-IR spectra of the starting material and of the samples A and C in the regions of 4000–400 and 1100–500 cm^{-1} (see inserted figure).

existence of hydroxyl groups and huge amount of water molecules in the surface and interlayer space. Vibration around 1637 cm^{-1} also confirmed the presence of water and can be assigned to H–O–H bending vibrations of water. The band around 897 cm^{-1} represents the stretching vibration of short Ti–O bonds involving nonbridging oxygen coordinated with sodium ions. As mentioned above, the peak for this band (~897 cm^{-1}) can be seen for sample A (marked with arrow in the inserted figure) and it could not be seen for sample C (hydrogen form). Since EDX analyses showed that there is no sodium ion present in sample C, hence we did not observe prominent form of above-mentioned band. For the comparison, the spectrum of TiO_2 sol has also been presented and it can bee seen from the figure that the FT-IR spectra of nanotubes (samples A and C) are apparently different than that of TiO_2. Neither of the bands obtained for the nanotubes can be ascribed to any known phase of TiO_2. On the basis of these FT-IR results, one can infer that the nanotubes contain huge amount of water, the sodium ions present in the samples are not only physically adsorbed but also belong to the lattice, and the composition is other than titanium dioxide.

3.2. Influence of calcination temperatures on the XRD patterns

The calcination temperatures may have significant effect on the phase, shape and morphology, BET surface area and other properties of the samples which in turn regulate the photocatalytic properties of the samples. Hence, this effect has been studied in which samples were calcined for 2 h at temperatures from 300 to 900 °C and change in phase and morphology was followed by using XRD and SEM analyses.

XRD patterns of the samples (samples A, B and C) calcined at different temperatures are shown in Figs. 3, 4 and 5, respectively. It can be seen from the Fig. 3 that the patterns are more or less similar up to 400 °C except that the intensity of diffraction peak near $2\theta \sim 10^{\circ}$ was decreased and shifted towards higher angle value indicating a decrease in interlayer distance for this plane. This contraction of layers may be due to the release of water molecules adsorbed and present in the spacings. The remaining diffraction peaks are slightly modified suggesting the maintenance of atomic structure in the temperature range 300–600 °C. The SEM analyses also confirmed that the drastic change (formation of rod like structures) occurred after 600 °C. On the other hand, at 700, 800 and 900 °C, emergence of new peaks took place. These new peaks can be assigned to sodium hexatitanates ($Na_2Ti_6O_{13}$) and sodium trititanates ($Na_2Ti_3O_7$) (PDF files for these are: 00-031-1329 for $Na_2Ti_3O_7$ and 00-037-0951 for $Na_2Ti_6O_{13}$). For the comparison, the reflections (bars) from $Na_2Ti_3O_7$ and $Na_2Ti_6O_{13}$ have also been provided in Fig. 3. The difference in relative intensities between XRD patterns for sodium tri- and hexatitanates and those reported for original samples may be

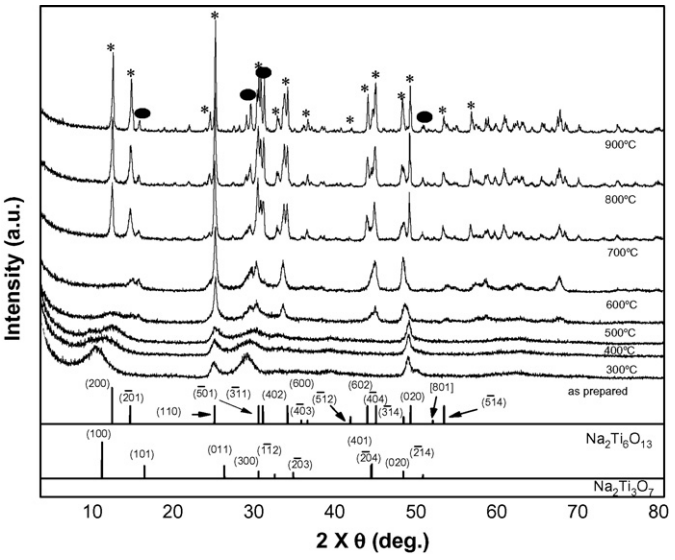

Fig. 3. XRD patterns of the sample A and of the samples obtained after calcination at different temperatures together with reflections (bars) from $Na_2Ti_3O_7$ and $Na_2Ti_6O_{13}$; (●) sodium trititanates and (*) sodium hexatitanates.

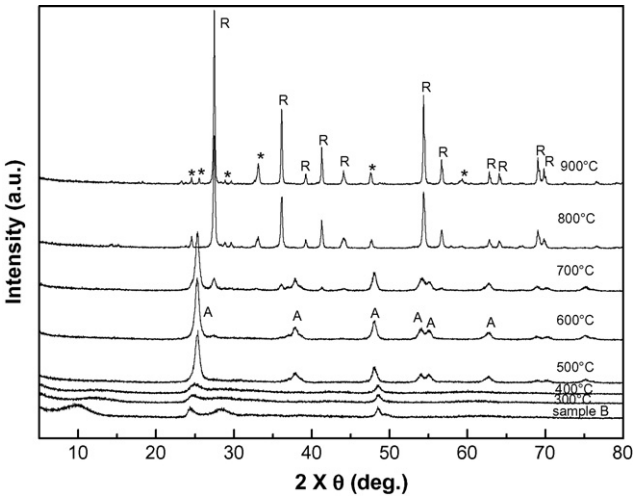

Fig. 4. XRD patterns of the sample B and of the samples obtained after calcination at different temperatures; (A) anatase, (R) rutile and (*) sodium hexatitanates.

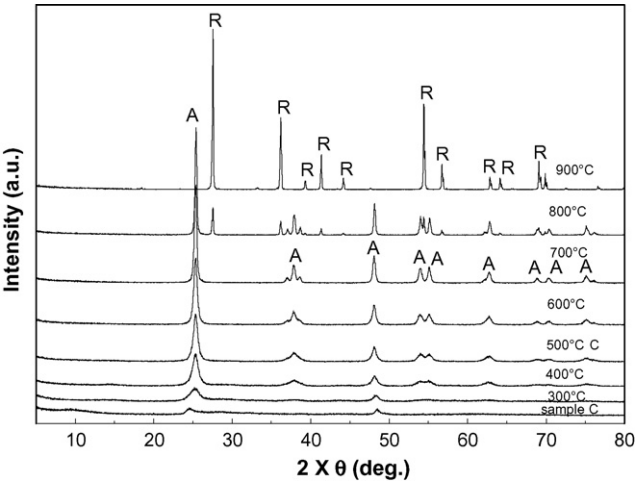

Fig. 5. XRD patterns of the sample C and of the samples obtained after calcination at different temperatures; (A) anatase and (R) rutile.

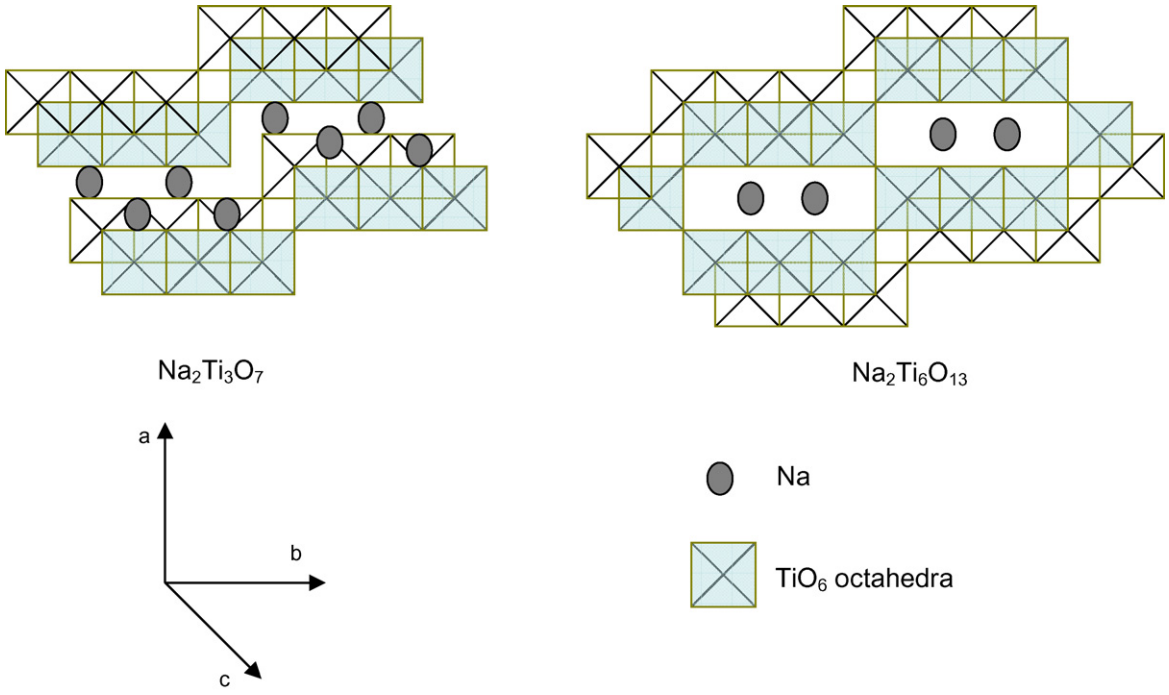

Scheme 1. Schematic representation showing the structural orientation of sodium tri- and hexatitanate.

attributed to the preparation conditions, shape and morphology, and particle size of the samples.

The presence of sodium hexatitanates phase in the thermal products is a crucial phenomenon in understanding the structural properties of the titanate nanotubes. It seems that at higher temperatures sodium trititanates undergo dimerization like process leading to the formation of sodium hexatitanates. The basic difference in the structures of sodium trititanates and sodium hexatitanates is that the former presents a lamellar structure with $Ti_3O_7^{2-}$ corrugated layers and two interlamellar Na^+ ions [39]. However, sodium hexatitanates shows a tunnel like structure with two Na^+ ions inside the tunnel. A schematic representation showing the difference in structural orientation in sodium tri- and hexatitanates has been shown in Scheme 1. From the structural point of view, the sharing of $Ti_3O_7^{2-}$ units of adjacent layers of $Na_2Ti_3O_7$ can give rise to tunnel like structure having two sodium ions inside [40]. In another study, Sauvet et al. [41] proposed that at higher temperatures the sodium trititanates tend to fuse and the formation of $Na_2Ti_6O_{13}$ is the result of ''Dimerization like'' process of $Na_2Ti_3O_7$. The presence of $Na_2Ti_6O_{13}$ in the thermal products can be considered as strong evidence that the structure and composition of as-prepared nanotubes are very similar to $Na_2Ti_3O_7$ and a general formula, on the basis of EDX, FT-IR and XRD results, for as-prepared nanotubes may be assigned as $Na_2Ti_3O_7{\cdot}nH_2O$. It is pertinent to mention here that any peak associated with TiO_2 could not be observed during heat treatment of the sample A indicating that the sample completely consisted of sodium titanates not anatase as claimed by many researchers. Another basis of the assignment of the trititanate composition for the as-prepared nanotubes is that neither of the chemical compositions and crystal structures proposed by other researchers, except trititanates, can lead to the formation of sodium hexatitanates upon heat treatment as a result of dimerization process. For example, since there are great structural similarities between $A_2Ti_4O_9$ and $A_2Ti_8O_{17}$ (A = Li, Na, K), the topotactic phase transition between $A_2Ti_4O_9$ and $A_2Ti_8O_{17}$ takes place owing to the condensation of corrugated layers [42]. It is noteworthy that the original samples of sodium trititanate also undergo dimerization or topotactic transition to yield sodium hexatitanate when heated at higher temperatures, as observed by Papp et al. [43] in a recent study.

Fig. 4 presents the XRD patterns of the sample B and its derivatives obtained at different temperatures. At 300 and 400 °C, the peak around 24° was found to shift to slightly higher value indicating the formation of anatase phase and complete transformation into anatase phase was obtained at 500 °C. Samples calcined at temperatures from 300 to 600 °C presented anatase phase, showing an increase in degree of crystallinity. The sample calcined at 700 °C has suffered a slight transformation of crystalline phase from anatase to rutile, being its phase composition about 89% anatase and 11% rutile. Whereas for the sample calcined at 800 °C, the anatase phase was completely transformed into rutile along with the formation of sodium hexatitanates ($Na_2Ti_6O_{13}$) in a small amount. However, at 900 °C, well-defined sodium hexatitanates appeared co-existing with rutile phase. It is pertinent to mention here that the sample B heated at 400 °C showed a slight formation of TiO_2 (B), a metastable monoclinic form of TiO_2, as shown in Fig. 6. The structure of TiO_2 (B) is consisted of edge- and corner-sharing of TiO_6 octahedra forming channel like structure. The appearance of TiO_2 (B) as intermediate product before complete crystallization into anatase eliminates the possibility of nanotubes being lepidocrocite type titanates because such kind of titanate first transforms into amorphous phase followed by the formation of anatase. The presence of

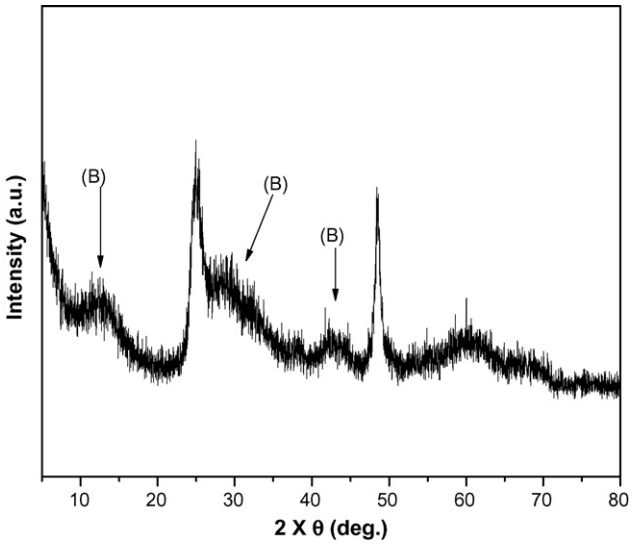

Fig. 6. XRD pattern showing the formation of TiO_2 (B) after heating the sample B at 400 °C.

TiO_2 (B), anatase, rutile phase and sodium hexatitanates in the thermal products of the sample containing medium amount of sodium ions clearly demonstrates that the basic crystal structure of the sample B is $Na_{2-x}H_xTi_3O_7{\cdot}nH_2O$ type depending on the extent of sodium ions exchanged with protons. The phenomenon (presence of TiO_2 phase and titanate phase) may be due to the presence of both the atoms such as protons as well as sodium ions. On the basis of these observations, it may be understood that at the initial temperatures the presence of protons in the sample facilitates the acid catalyzed condensation of OH groups present into the interstitial spacings between the layers during heat treatment. However, at higher temperatures, where the sodium ions were present in the sample tend to dimerize resulting in the formation of sodium hexatitanates. Few other researchers also noted the formation of anatase, rutile and sodium hexatitanates in the thermal products [43–46].

Our assumption that the basic crystal structure of the nanotubes is very close to trititanate was being further supported when the sample C (free from sodium) was heated at different calcination temperatures. The changes in XRD patterns of the sample C followed by calcination at different temperatures are shown in Fig. 5. In this case, we only obtained the phases of TiO_2 such as anatase and rutile without any titanates within the temperature range studied. The XRD improvement patterns as a function of calcination temperatures were not much different than that of sample B besides the presence of sodium hexatitanates in the thermal products at higher temperatures. Unlike the sample B, sample C showed the formation of TiO_2 (B) at 300 °C and this variation in results may be attributed to the small amount of sodium ions present in the sample B which slightly stabilizes the sample. The quantity of sodium ions present in the samples plays a crucial role in the stability and phase transformation of the nanotubes. The XRD patterns obtained after heating the sample C clearly show a condensation and structural transformation of $Ti_3O_7^{2-}$ into TiO_2 (B), anatase and finally rutile phase. These structural changes may be again rationalized in terms of fact that, in an ion-exchange process, the protons replaced the sodium ions completely and facilitates the acid catalyzed condensation of OH groups during heat treatment and lead to the formation of TiO_2 according to the following equation:

$$H_2Ti_3O_7 \rightarrow 3TiO_2 + H_2O$$

On the basis of these observations, it may be inferred that the composition and structure of the sample C is very similar to layered protonic titanates and a general formula may be assigned as $H_2Ti_3O_7{\cdot}nH_2O$.

Our results obtained in this study clearly indicate that the structure of samples A (as-prepared), B (moderately washed with acid) and C (thoroughly washed with acid) is $Na_2Ti_3O_7{\cdot}nH_2O$, $Na_{2-x}H_xTi_3O_7{\cdot}nH_2O$ (depending on the degree of proton exchange) and $H_2Ti_3O_7{\cdot}nH_2O$, respectively.

3.3. Influence of acid washing and calcination temperatures on the shape and morphology

Transmission electron micrographs (TEM) of the nanotubes, samples A, B and C, were also collected. When the TEM micrographs of the samples A, B and C were compared, we did not observe any obvious difference in diameters or lengths of the nanotubes. As a representative example, TEM micrographs for sample A have been presented in Fig. 7(a) and (b). From the TEM images, the outer and the inner diameters of the tubes

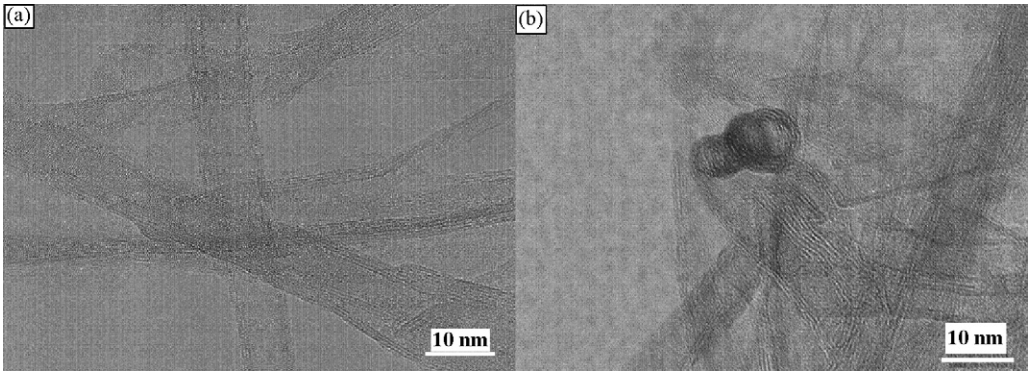

Fig. 7. Transmission electron micrographs of (a) as-prepared nanotubes (viewed along the axis), (b) as-prepared nanotubes showing the cross-sectional view.

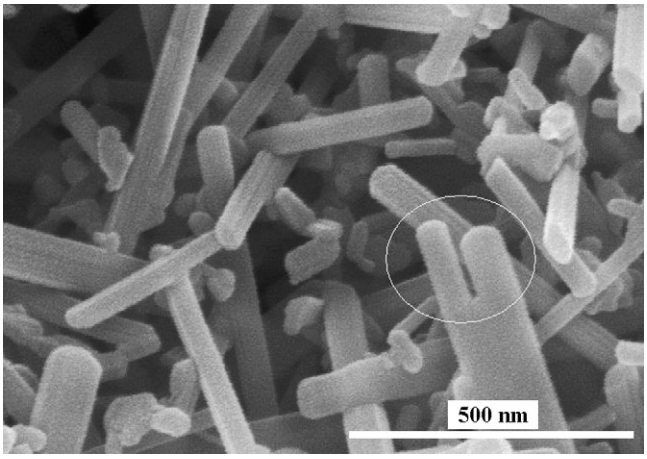

Fig. 8. SEM micrographs showing the fusion process of the sample A at 700 °C.

were measured to be about 6–10 and 4–6 nm, respectively, and the lengths were measured to be several hundreds of nanometers. All the nanotubes are open at both ends and multilayered. Fig. 7(b) represents the non-seamless open end of the multiwalled nanotubes. Our results essentially contradict the theory that nanotubes can only be obtained after washing with acid. TEM and SEM analyses indicated that a large number of pure nanotubes can be obtained without any acid treatment indicating that the driving force for the formation of nanotubes are highly basic conditions and high process temperature rather than acid treatment.

The change in shape and morphology of the samples A, B and C occurred with respect to calcination temperature was followed by using SEM analyses technique. SEM results of sample A indicated that the morphology of the nanotubes were not much affected up to 500 °C and when the calcination temperature was raised to 700 °C, the samples were found to fuse with each other and completely transformed into rod-shaped nanoparticles or one-dimensionally connected nanostructure. The process of fusion with each other has been well captured by SEM and shown in Fig. 8. The SEM results are also consistent with XRD results that the patterns drastically changes after 600 °C. These rods or one-dimensionally connected nanoparticles may be very useful from engineering point of view.

The microstructures of the hexatitanate rods formed at 700 °C after heating the sample A for 2 h were also analyzed by TEM and the micrographs obtained are shown in Fig. 9(a) and (b). The diameter of the nanorod was about 25–30 nm with several hundred nanometers in length. High-resolution micrographs (Fig. 9 (b)) revealed that the nanorods consisted of two lattice fringes of 6.3 and 3.6 Å spacings. The lattice fringe 6.3 Å was parallel to the nanorods and the angle between two fringes was about 80°. Similar kind of nanorods consisted of hexatitanate structures were also obtained by other researchers [27,44].

The shape and morphology of sample B calcined at various temperatures were not found to be much different than that of sample C. TEM micrograph and corresponding selected area electron diffraction (SAED) patterns of the sample C heated at 600 °C have been shown in Fig. 10(a) and (b), respectively. Surprisingly, TEM image indicated that the tubular morphology of the sample was completely lost and transformed into grain like nanoparticles (15–30 nm) rather than rod-like or one-dimensionally connected structures (seen in case of sample A) during the heat treatment of samples B and C. On the other hand, the ED patterns of the sample C calcined at 600 °C clearly indicated that the formed phase of the powder is anatase rather than any titanate. Sample C heated at 900 °C was also analyzed by TEM and the obtained TEM image and corresponding SAED patterns have been shown in Fig. 11(a) and (b), respectively. It can be seen from the Fig. 11(a) that the size of the grain like nanoparticles has increased up to several hundreds nanometer due to the high temperature. ED patterns (Fig. 11(b)) indicated that the phase of the nanoparticles obtained at 900 °C is polycrystalline rutile, as it was also evidenced by the XRD patterns. Furthermore, the samples B and C began to loose the morphology at somewhat lower temperatures such as 500 °C. The presence of proton in acid-treated samples will explain this behavior.

3.4. Influence of calcination temperature on the specific surface area

The effect of acid washing and heat treatment at different temperatures from 300 to 900 °C on the BET surface area of the samples A, B and C was studied and the results obtained are depicted in Table 1. The surface areas of the different samples

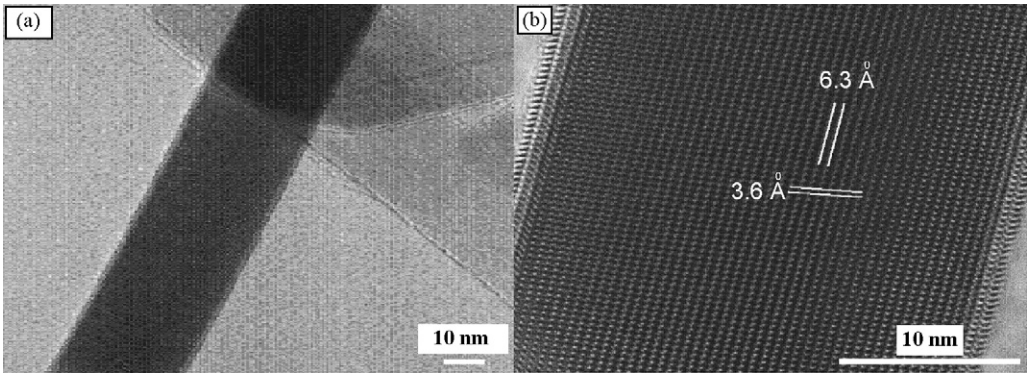

Fig. 9. Transmission electron micrographs of (a) nanorod (obtained by calcination of sample A at 700 °C) and (b) enlarged part of the nanorod.

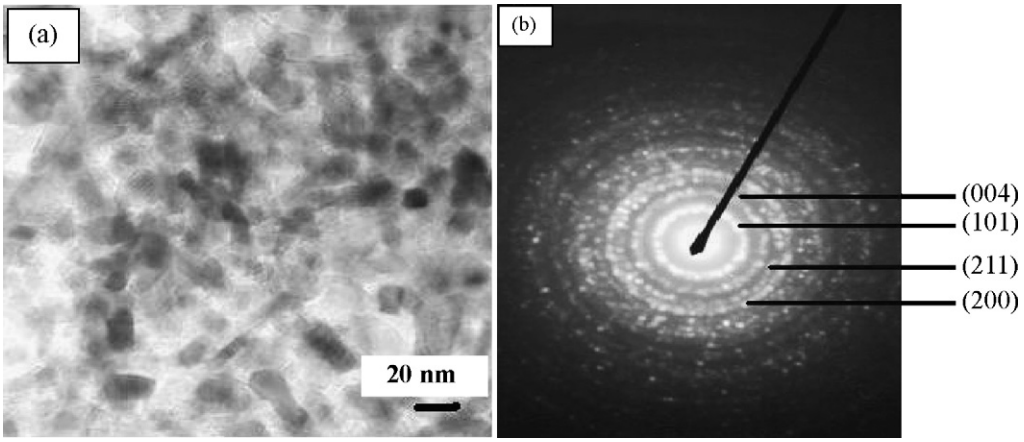

Fig. 10. Transmission electron micrograph (a) and selected area electron diffraction (SAED) pattern (b) of the sample C calcined at 600 °C.

are found to be strongly influenced by acid washing and heat treatment. The surface area showed distinct values depending on the sodium contents in the composition and acid washing was favorable to increase the surface area of the samples i.e., lower is the sodium contents, higher is the specific surface area. Sodium trititanate and hydrogen trititanate have specific surface areas of 254.0 and 353.3 $m^2\,g^{-1}$, respectively. However, the surface area of $Na_{2-x}H_xTi_3O_7{\cdot}nH_2O$ was (329.34 $m^2\,g^{-1}$) in between the value of above-mentioned two phases. Owing to the smaller size of H^+ ions, present in hydrogen trititanates, a higher adsorption of nitrogen gas (during the analysis of BET surface area) on the external surface and between the layers may be expected and, hence, a larger surface area was obtained. The decrease in the surface area with the increasing temperature may be rationalized in terms of the fact that as we increase the temperature, the pores and/or interlayers of the nanotubes collapse (transformation of tubes into rod like structure) and, hence, less adsorption of nitrogen gas on nanotubes may be expected and this phenomenon can lead to decrease in surface area of the powder. As depicted in Table 1, the surface area is highly decreased at higher temperatures, this fact may be collectively attributed to different factors, such as formation of rod like structures (complete loss of porosity), formation of rutile, sintering effect and growth of crystallites.

3.5. Influence of calcination temperature on the photocatalytic activity

The photocatalytic activity of samples A, B and C and their thermal derivatives obtained after heating at different calcination temperatures from 300 to 900 °C have been evaluated using the photooxidation of amaranth as probe reaction. Photonic efficiencies obtained for the degradation of amaranth in the presence of different samples have been depicted in Table 1. The results indicated that as-prepared or acid washed samples of the nanotubes showed no photocatalytic activity at all. Our results essentially contradict those reports in which the as-prepared nanotubes have been shown to be highly potential photocatalysts for the destruction of organic contaminants. For example, Xu et al. [32] claim that the as-prepared nanotubes showed higher photocatalytic activity even than Degussa P25 for the degradation of acetaldehyde. However, no information has been given about the crystal structure and composition of the nanotubes. On the other hand, Nakahira et al. [21] reported that the crystal structure of nanotubes is $H_2Ti_4O_9{\cdot}H_2O$ and

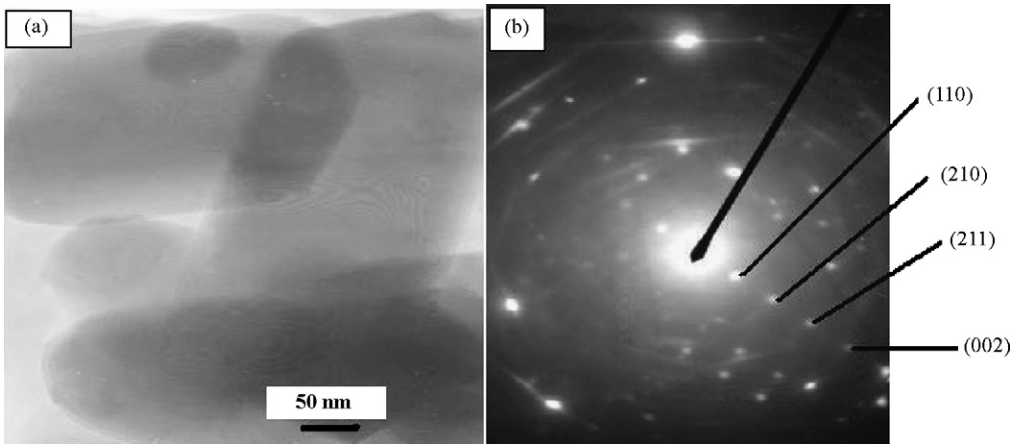

Fig. 11. Transmission electron micrograph (a) and selected area electron diffraction (SAED) pattern (b) of the sample C calcined at 900 °C.

Table 1
Calcination temperatures, anatase crystallite sizes, BET surface area and percent photonic efficiency of amaranth for the samples A, B and C

Sample	Calcination temperature (°C)	Anatase crystallite size (nm)	BET surface area (m^2/g)	Photonic efficiency (mole $S^{-1} \times m^{-3}$)
Sample A	0	–	254.00	–
	300	–	225.08	–
	400	–	187.83	–
	500	–	123.42	– –
	600	–	78.210	– –
	700	–	46.190	– –
	800	–	27.780	– –
	900	–	11.530	– –
Sample B	0	–	329.34	– –
	300	3.620	252.61	0.1302
	400	6.220	192.18	0.2274
	500	11.45	109.09	0.3073
	600	20.29	72.640	0.1806
	700	38.48	32.530	0.0972
	800	Rutile	21.110	0.0208
	900	Rutile	04.210	0.0052
Sample C	0	–	353.30	– –
	300	4.020	268.49	0.1667
	400	10.21	185.54	0.4635
	500	16.82	106.23	0.3403
	600	26.31	70.050	0.2292
	700	40.78	34.790	0.1284
	800	52.63	22.000	0.0347
	900	Rutile	7.0600	0.0087
Degussa P25		20–25	50.000	0.5833

–, Anatase is absent in the phase.
– –, Photonic efficiency is nearly zero.

found that the photocatalytic property of as-prepared nanotubes is higher than that of water washed nanotubes and Degussa P25. This high photocatalytic activity was explained in terms of higher surface area that was 160 $m^2\ g^{-1}$. In contrast, Khan et al. [31] insist that the nanotubes consist of anatase structure and the photocatalytic property of as-prepared nanotubes were lower than those in which sodium was exchanged by protons and this ion-exchange reaction was first performed with acid and finally in presence of hydrogen peroxide. It was concluded that this higher photocatalytic activity of H_2O_2-treated nanotubes was due to Bronsted acidity induced by protons. Moreover, the surface area of as-prepared nanotubes was found to be 97.9 $m^2\ g^{-1}$ and when the sodium was exchanged with protons, the value was decreased from 97.9 to 93.0 $m^2\ g^{-1}$. This result is unlikely because the size of the proton is smaller than that of sodium and when the sodium is exchanged with protons, some interlayer spaces remain available for the adsorption of nitrogen gas, during the analyses of specific surface area, that is responsible for higher surface area. Many researchers have discussed this phenomenon and found that the surface area was greatly increased as the sodium was exchanged with protons [21,43–45].

From the Table 1, it can be seen that the photonic efficiencies of the amaranth is greatly affected by the calcination temperatures of the samples containing different amounts of sodium ions or, in other words, consisting of different phases and crystallinity. The degradation of the dye in presence of thermal products of samples B and C drastically increases following the change in phase, however, the degradation remained unchanged in the presence of different calcined products obtained from sample A. These results also support the theory that the as-prepared or acid-treated nanotubes are consisted of titanate structures rather than any known phase of TiO_2 (anatase) as claimed by many researchers.

It can be observed from the Table 1 and also Figs. 12 and 13 that the photocatalytic activity of samples B and C increases with increasing calcination temperature, presumably due to the formation of anatase phase and improvement of its crystallinity, and the samples calcined at 400 and 500 °C showed the best activities for the degradation of the dye followed by a decrease at higher temperatures. The high photocatalytic activity shown by samples calcined at 400 and 500 °C seems to be due a compromise between the surface area and degree of crystallinity. On the other hand, the low activity shown by the samples (samples B and C) calcined at 300 °C compared to 400 and 500 °C calcined samples could be due to its poor degree of crystallinity and smaller fraction of anatase phase attained, which is not compensated by the positive effect given by its high surface area. The decrease in photocatalytic activity of the samples at higher temperatures could be explained by the strong decrease in surface area, together with the loss of anatase phase, observed in the samples with the increase of the calcination temperatures.

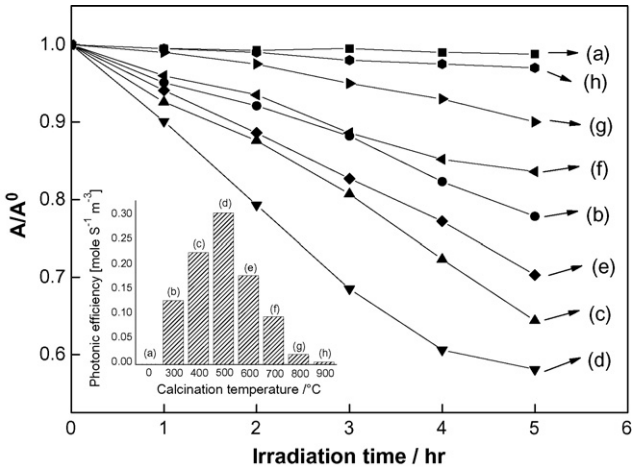

Fig. 12. Photocatalytic degradation of amaranth in the presence of sample B calcined at different temperatures for 2 h: (a) sample B, (b) 300 °C, (c) 400 °C, (d) 500 °C, (e) 600 °C, (f) 700 °C, (g) 800 °C and (h) 900 °C. Inserted figure: percent photonic efficiency. Experimental conditions: dye concentration (0.15 mM), $V = 500\ cm^3$, catalysts concentration ($1\ g\ l^{-1}$), irradiation time = 5 h.

When the degradation of the amaranth obtained in presence of different calcined products of the samples B and C was compared, the highest photocatalytic activity was observed in the presence of the thermal products obtained from sample C, as shown in Figs. 12 and 13, respectively. This phenomenon is in accordance with the change in crystal structures as a function of temperature. As mentioned above, when the sample A was heated at higher temperatures it transformed into sodium hexatitanates and some parts still remained as trititanates and, therefore, the degradation of the dye remain unchanged. Whereas, the sample containing 1.09 wt% sodium ions (sample B) was first transformed into anatase at initial temperatures followed by rutile formation and, at higher temperatures, such as 900 °C, a mixture of rutile and hexatitanates was obtained. However, in case of sample C, only anatase and rutile phase were obtained indicating that a complete exchange of sodium with protons were achieved. The variation in photocatalytic activities of the different heated samples (samples B and C) may be explained in terms of the fact that, in case of sample B, some sodium ions were exchanged with protons and these exchanged protons are responsible for the acid catalyzed condensation of OH groups present into the interstitial spacings between layers and lead to the formation of anatase phase. However, some parts of the sample B, where the sodium was present remained as trititanate and appeared as hexatitanates at higher temperature. On the other hand, in case of sample C, entire amount of the sample was transformed into anatase phase. Consequently, this phenomenon led to a slightly higher photocatalytic activity of calcined sample C than that of sample B i.e. the larger is the fraction of active anatase, the higher is the photocatalytic activity.

The photocatalytic activity of the sample C calcined at 400 °C was compared with the activity of Degussa P25, a widely used commercial TiO_2. The corresponding profiles for the degradation of amaranth have been shown in Fig. 14. The photocatalytic activity of sample C calcined at 400 °C was found to be slightly lower than that of Degussa P25. This may be due to the fact that the phase of sample C is trititanate and when the sample was heated at different temperatures, phase gradually changes to anatase leading to generation of photocatalytic properties in samples. No sooner, the sample's photocatalytic activity increases following the change in structure than the temperature began to induce negative effects on the photocatalytic property by increasing the particle size and decreasing the surface area. On the other hand, the higher photocatalytic activity of Degussa P25 may be due to its mixed phase (70% anatase and 30% rutile). The excited electrons are being trapped in interwoven rutile phase thus inhibiting the electron-hole pair recombination which in turn increases the photocatalytic efficiency of the P25. The decrease in photocatalytic activity of sample C at higher temperatures

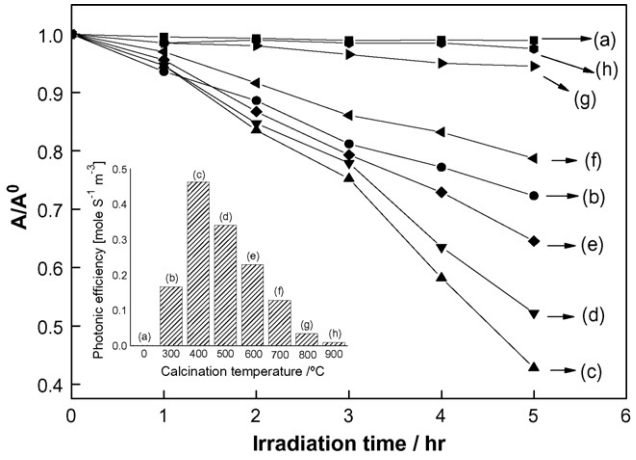

Fig. 13. Photocatalytic degradation of amaranth in the presence of sample C calcined at different temperatures for 2 h: (a) sample C, (b) 300 °C, (c) 400 °C, (d) 500 °C, (e) 600 °C, (f) 700 °C, (g) 800 °C and (h) 900 °C. Inserted figure: percent photonic efficiency. Experimental conditions: dye concentration (0.15 mM), $V = 500\ cm^3$, catalysts concentration ($1\ g\ l^{-1}$), irradiation time = 5 h.

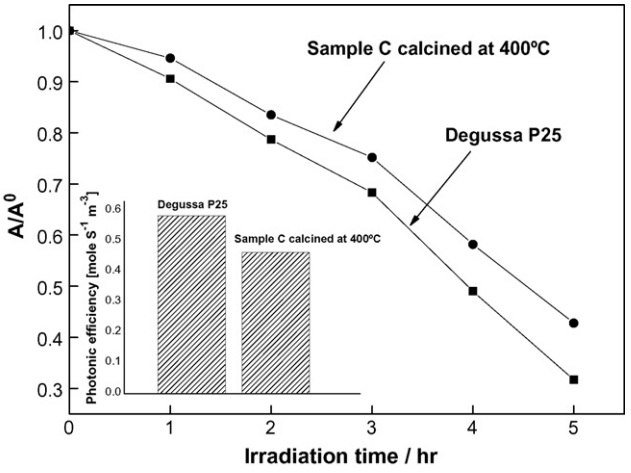

Fig. 14. Comparison of photocatalytic degradation of amaranth in the presence of Degussa P25 and sample C calcined at 400 °C for 2 h. Inserted figure: percent photonic efficiency. Experimental conditions: dye concentration (0.15 mM), $V = 500\ cm^3$, catalysts concentration ($1\ gL^{-1}$), irradiation time = 5 h.

may collectively be attributed to different factors, such as growth of crystallite size, sintering, decrease in surface area, and formation of rutile phase, which are very crucial to regulate the photocatalytic activity of a sample.

The present study of the photocatalytic behavior of the nanotubes suggested that as-prepared samples (sodium or protonic form) did not show any photocatalytic activity and hence cannot be used as a photocatalsyst for the destruction of organic pollutants because they are consisted of titanate phase rather than any known phase of TiO_2. On the other hand, when the nanotubes sample free from sodium ions was calcined at some temperatures, the titanate phase was found to crystallize into anatase phase and this change in structure from titanate to anatase generates photocatalytic activity in the nanotubes samples. The observed photocatalytic activity in the nanotubes samples was all due to the formation of anatase phase rather than titanate phase.

Based on the this study, it may be inferred that the particle size and surface area of a single phase, when it has been obtained by calcination in particular, play very crucial role in determining the photocatalytic activity of the samples. Generally, there exist an optimum combination between the particle size and surface area of the samples for higher photocatalytic activity. For example, the particle size and surface area of the sample C heated at 300 °C was found to be 4.020 nm and 268.49 $m^2\ g^{-1}$, respectively. When the sample C was heated at 400 °C the particle size was increased (10.21 nm) whereas the surface area was decreased (185.54 $m^2\ g^{-1}$) and this trend continued with the increasing calcination temperature. However, the highest photocatalytic activity was observed for the sample C heated at 400 °C. This may be due to the fact that when the particle size of the sample is very small and the surface area is large, the reactive sites formed on the surface of the catalyst are adequate to absorb the organic pollutants i.e. the higher is the adsorption, the higher is the surface reaction. On the other hand, at the same time, since the electron-hole pair recombination rate is mostly determined by the quantity of surface defects, it is thought that greater surface reactivity is diminished by the high recombination rate of photo-excited charge carriers which is more efficient in these quantum sized particles [47–52]. Wang et al. [53] performed a study based on the relation between particle size and photocatalytic activity of the samples and found that the higher particle size and lower surface area (21 nm, 70 $m^2\ g^{-1}$) as well as lower particle size and higher surface area (6 nm, 253 $m^2\ g^{-1}$) of the samples were unfavorable for its photocatalytic properties and the samples with intermediate grain size and surface area (11 nm, 157 $m^2\ g^{-1}$) showed the highest photocatalytic activity. The higher photocatalytic activity, therefore, may be achieved at the point where the optimum compromise between surface area and particle size occurred for a pure nanocrystalline TiO_2.

Our results dealing with the photocatalytic properties of nanotubes and its thermal products are in good agreements with the results obtained by Zhang et al. [34] but essentially contradicts the results obtained by Yu et al. [35], in which, the photocatalytic activity of the nanotubes calcined at 400 and 500 °C was shown to be 3.0 times higher than that of Degussa P25.

Some of the possible reasons in variation of results regarding the photocatalytic activity may be synthetic conditions of the nanotubes and/or the model pollutants chose for the photocatalytic study. With this view, the nanotubes were also synthesized under different synthetic temperatures such as 130 and 110 °C by keeping the heating time constant. Since the highest photocatalytic properties were obtained in the presence of those calcined samples which were free from sodium ions, the sodium ions of the samples obtained at different synthetic temperatures were completely removed and calcined at 400 and 500 °C. The photocatalytic properties of these newly synthesized samples were investigated under identical conditions for the degradation of amaranth. When the photocatalytic activity of different samples was compared, the change in photonic efficiency was not noticeable. These findings suggest that the photocatalytic property of nanotubes is not much affected by its synthetic temperatures.

The photocatalytic property of sample C calcined at 300–500 °C was also investigated under similar conditions for the degradation of two other pollutants, such as 4-chlorophenol and methylene blue by considering the selectivity of the catalysts towards the contaminants. The degradation patterns for the 4-chlorophenol were more or less similar; the photocatalytic activity increases with the increase in calcination temperatures up to 400 °C followed by decrease at 500 °C. When the photonic efficiency of 4-cholorophenol obtained in the presence of sample C calcined at 400 °C was compared with that of Degussa P25, P25 again showed better photocatalytic activity.

It is pertinent to mention here that when the methylene blue was used as model pollutant, a high degree of adsorption of the dye was observed (nearly 70%) in the dark on the surface of the sample C, presumably due to the higher surface area. The degradation kinetics, therefore, could not be studied for this model pollutant because the degradation rates obtained in this case would not be the actual rates.

4. Conclusion

Nanotubes were successfully obtained directly from a TiO_2 sol following a hydrothermal process in the presence of sodium hydroxide with and without acid washing. We have shown that the nanotubes contain huge amount of water, sodium (belongs to lattice) and consisted of trititanate structure with formula $Na_2Ti_3O_7{\cdot}nH_2O$, $Na_{2-x}H_xTi_3O_7{\cdot}nH_2O$ and $H_2Ti_3O_7{\cdot}nH_2O$ where x is dependant on the washing process with acid. The study of thermal products indicated that the sample containing sodium ions transforms into sodium hexatitanates, while hydrogen trititanate showed the formation of anatase and rutile phase involving the TiO_2 (B) as intermediate. Different experimental evidences revealed that the products of desired phase (tri- and hexatitanates, TiO_2 (B) and anatase) and desired morphology (rod-like structure or nanoparticles) can be successfully achieved by controlled post treatments. The as-prepared nanotubes were found to be inert towards photocatalytic reactions. The photocatalytic activity of the samples was highly dependant on the amount of sodium ions and was

found to increase when acid-treated nanotubes were calcined at different temperatures following the formation of active anatase phase.

Acknowledgment

This work was supported by the faculty research fund of Sejong University in 2006.

References

[1] P. Wang, S.M. Zakeeruddin, J.E. Moser, M.K. Nazeeruddin, T. Sekiguchi, M. Gratzel, Nat. Mater. 2 (2003) 402.
[2] A. Hagfeldt, M. Gratzel, Chem. Rev. 95 (1995) 49.
[3] Z.-R. Tian, W. Tong, J.-Y. Yong, N.-G. Duan, V.V. Krishnan, S.L. Suib, Science 276 (1997) 926.
[4] S. Matsuda, Appl. Catal. 8 (1983) 149.
[5] Y.C. Yeh, T.T. Tseng, D.A. Chang, J. Am. Ceram. Soc. 73 (1990) 1992.
[6] Y.K. Zhou, L. Cao, F.B. Zhang, B.L. He, H.L. Li, J. Electrochem. Soc. 150 (2003) A1246.
[7] C.-C. Wang, J.Y. Ying, Chem. Mater. 11 (1999) 3113.
[8] N. Negishi, K. Takeuchi, T. Ibusuki, J. Mater. Sci. Lett. 18 (1999) 515.
[9] N. Ulagappan, C.C.R. Rao, Chem. Commun. 14 (1996) 1685.
[10] H. Hoyer, Langmuir 12 (1996) 141.
[11] H. Imai, Y. Takei, K. Shimizu, M. Matsuda, H. Hirashima, J. Mater. Chem. 9 (1999) 2971.
[12] T. Kasuga, M. Hiramatsu, A. Hoson, T. Sekino, K. Niihara, Langmuir 14 (1998) 3160.
[13] S. Zhang, J. Zhou, Z. Zhang, Chin. Sci. Bull. 45 (2000) 1533.
[14] Q. Chen, W. Zhou, G. Du, L.M. Peng, Adv. Mater. 14 (2002) 1208.
[15] A.L. Ivanoskii, Russ. Chem. Rev. 71 (2002) 175.
[16] S. Kobayashi, K. Hanabusa, N. Hamasaki, M. Kimura, H. Shirai, S. Shinkai, Chem. Mater. 12 (2000) 1523.
[17] D. Gong, C.A. Grimes, O.K. Varghese, W. Hu, R.S. Singh, Z. Chen, E.C. Dickey, J. Mater. Res. 16 (2001) 3331.
[18] G.H. Du, Q. Chen, R.C. Che, Z.Y. Yuan, L.M. Peng, Appl. Phys. Lett. 79 (2001) 3702.
[19] A. Thorne, A. Kruth, D. Tunstall, J.T.S. Irvine, W.J. Zhou, J. Phys. Chem. B 109 (2005) 5439.
[20] Q. Chen, G.H. Du, S. Zhang, L.M. Peng, Acta Crystallogr. 19 (2004) 417.
[21] A. Nakahira, W. Kato, M. Tamai, T. Isshiki, K. Nishio, J. Mater. Sci. 39 (2004) 4239.
[22] R. Ma, Y. Bando, T. Sasaki, Chem. Phys. Lett. 380 (2003) 577.
[23] R. Ma, K. Fukuda, T. Sasaki, M. Osada, Y. Bando, J. Phys. Chem. B 109 (2005) 6210.
[24] Y. Suzuki, S. Yoshikawa, J. Mater. Res. 19 (2004) 982.
[25] X. Sun, Y. Li, Chem. Eur. J. 9 (2003) 2229.
[26] D.V. Bavykin, V.N. Parmon, A.A. Lapkin, F.C. Walsh, J. Mater. Chem. 14 (2004) 3370.
[27] R. Yoshida, Y. Suzuki, S. Yoshikawa, Mater. Chem. Phys. 91 (2005) 409.
[28] J. Yang, Z. Jin, X. Wang, W. Li, J. Zhang, S. Zhang, X. Gao, Z. Zhang, Dalton Trans. (2003) 3898.
[29] B.D. Yao, Y.F. Chan, X.Y. Zhang, W.F. Zhang, Z.Y. Yang, N. Wang, Appl. Phys. Lett. 82 (2003) 281.
[30] Q. Zhang, L. Gao, L. Sun, S. Zheng, Chem. Lett. 2 (2002) 226.
[31] M.A. Khan, H.T. Jung, O.B. Yang, J. Phys. Chem. B 110 (2006) 6626.
[32] H. Xu, G. Vanamu, Z. Nie, J. Phillips, Y. Yang, Mater. Res. Soc. Symp. Proc. (2005) 876E.
[33] H. Zhu, X. Gao, Y. Lan, D. Song, Y. Xi, J. Zhao, J. Am. Chem. Soc. 126 (2004) 8380.
[34] M. Zhang, Z. Jin, J. Zhang, X. Guo, J. Yang, W. Li, X. Wang, Z. Zhang, J. Mol. Catal. A Chem. 217 (2004) 203.
[35] J. Yu, H. Yu, B. Cheng, C. Trapalis, J. Mol. Catal. A Chem. 249 (2006) 135.
[36] B. Wen, C. Liu, Y. Liu, Z. Zhang, J. Nanosci. Nanotechnol. 4 (2004) 1062.
[37] M. Hodos, E. Horvath, H. Haspel, A. Kukovecz, Z. Konya, I. Kiricsi, Chem. Phys. Lett. 399 (2004) 512.
[38] S.J. Kim, K. Lee, J.H. Kim, N.H. Lee, S. Jin Kim, Mater. Lett. 60 (2006) 364.
[39] O.V. Yakubovich, V.V. Kirrev, Crystallogr. Rep. 48 (2003) 24.
[40] G.W. Peng, S.H. Leu, Mater. Chem. Phys. 42 (1995) 264.
[41] A.L. Sauvet, S. Baliteau, C. Lopez, P. Fabry, J. Solid State Chem. 177 (2004) 4508.
[42] R. Marchand, L. Brohan, M. Tournoux, Mater. Res. Bull. 15 (1980) 1129.
[43] S. Papp, L. Korosi, V. Meynen, P. Cool, E.F. Vansant, I. Dekany, J. Solid State Chem. 178 (2005) 1614.
[44] E. Morgado Jr, M.A.S. De Abreu, O.R.C. Pravia, B.A. Marinkovic, P.M. Jardim, F.C. Rizzo, A.S. Araujo, Solid State Sci. 8 (2006) 888.
[45] P. Poudel, W.Z. Wang, C. Dames, J.Y. Huang, S. Kunwar, D.Z. Wang, D. Banerjee, G. Chen, Z.F. Ren, Nanotechnology 16 (2005) 1935.
[46] C.C. Tsai, H. Teng, Chem. Mater. 18 (2006) 367.
[47] H. Kominami, S. Murakami, J. Kato, Y. Kera, B. Ohtani, J. Phys. Chem. 106 (2002) 10501.
[48] D.W. Bahnemann, S.N. Kholuiskaya, R. Dillert, A.I. Kulak, A.I. Kokorin, Appl. Catal. B Environ. 36 (2002) 161.
[49] A.J. Maira, K.L. Yeung, C.Y. Lee, P.L. Yue, C.K. Chan, J. Catal. 192 (2000) 185.
[50] J.M. Coronado, A.J. Maira, J.C. Conesa, K.L. Yeung, V. Augugliaro, J. Soria, Langmuir 17 (2001) 5368.
[51] K.L. Yeung, A.J. Maira, J. Stolz, E.W.C. Hung, N.K.C. Ho, A.-C. Wei, J. Soria, K.-J. Chao, P.-L. Yue, J. Phys. Chem. B 106 (2002) 4608.
[52] K.L. Yeung, S.T. Yau, A.J. Maira, J.M. Coronado, J. Soria, P.L. Yue, J. Catal. 219 (2003) 107.
[53] C.C. Wang, Z. Zhang, J.Y. Ying, Nanostruct. Mater. 9 (1997) 583.